ACS OMEGA

Open Access

http://pubs.acs.org/journal/acsodf

Article

Binary Doping of Strontium−Magnesium to Bioactive Glasses to Enhance Antibacterial and Osteogenic Effects

Zhige Li,[#] Ziyuan Li,[#] Jiao Wang,[#] Lingzi Liao, Xinjie Li, Zhidong Zhang, Xin Yang, Xiangxue Yu, Baoquan Fan, Bo Li,[*] Jun Hai,[*] and Baoping Zhang[*]

Cite This: *ACS Omega* 2025, 10, 215−229

Read Online

ACCESS | Metrics & More | Article Recommendations | Supporting Information

ABSTRACT: Bone defects that exceed the critical defect value, resulting from fractures and diseases, are often difficult to heal. Although bone tissue engineering is a promising treatment for extensive osseous defects, orthopedic-implant-related infections increase the likelihood of failure. Bioactive glass (BG) has been widely used in the manufacture of artificial bone scaffolds, owing to its excellent biocompatibility and osteoinductivity. Nevertheless, considering that infection conditions and trauma can affect the osteogenic capacity of bioactive glass, this study combined BG with magnesium and strontium to promote osteogenesis and confer significant antimicrobial activity. Novel bioactive glass doped with magnesium−strontium (BGMSN) with good biocompatibility, excellent antibacterial properties, and promising osteogenic induction ability was constructed from 45S5, Mg, and Sr carbonates via a melt-quenching approach. The results of an *in vitro* cell biocompatibility study indicated that the BGMSN exhibited good cellular compatibility. Furthermore, osteogenic alkaline phosphatase, osteocalcin, and osteopontin genes were upregulated upon BGMSN/MC3T3-E1 coculture. BGMSN exhibited potent *in vitro* antibacterial effects against *Staphylococcus aureus*, *Escherichia coli*, and *Streptococcus mutans*. Animal experiments further demonstrated the exceptional bone-inducing ability of BGMSN. Accordingly, owing to their excellent antimicrobial properties, BGMSN can be used for bone regeneration, particularly under infected conditions.

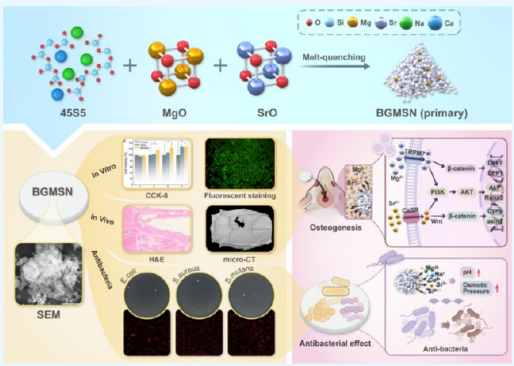

1. INTRODUCTION

Bone defects induced by tumors, severe infections, osteoporosis, osteonecrosis, and certain congenital malformations are currently among the principal causes of disability and ultimately lower the quality of life.[1,2] Consequently, the repair and functional reconstruction of bone defects have become important research topics worldwide. More specifically, various implantable biomaterials have been developed, including cell-based products,[3] new intelligent micro−nanomaterials, modular fabrications, and three-dimensional (3D) and four-dimensional (4D) printed materials.[4] Although bone regeneration using such materials shows excellent promise, they are associated with high costs, a potential risk of tumor growth, and an inability to naturally combine with the surrounding healthy tissue. Moreover, orthopedic-implant-associated infections, which are mainly caused by *Staphylococcus aureus* (*S. aureus*), can further affect bone regeneration and remain an ongoing challenge.[5] In this context, repeated antibiotic treatment increases the possibility of drug resistance, with 40% of pathogenic *S. aureus* strains being methicillin-resistant; therefore, the inherent antibacterial abilities of such implants should also be considered.

Biocompatible ceramics exhibit remarkable chemical similarities to human hard tissues and are ideal for use in replacement surgeries. Their greatest advantage is that they are gradually degraded by solution-driven and cell-mediated processes after implantation in the body and are finally replaced by new lamellar bone tissue.[6] However, *in vivo* studies have shown that the dissolution of calcium ions and soluble silica from bioactive glass (BGs) stimulates osteoblast cell division, production of growth factors, and mimicking natural extracellular matrix. This leads to bioactive glasses bonding with bone more rapidly than other bioceramics.[7,8] BGs are synthetic silica-based biomaterials and are well established for applications involving bone regeneration and repair.[7] Previous studies have reported the synthesis, characterization, and biological behavior of 45S5 BG, which is composed of 45 mol % SiO_2, 24.5 mol % CaO, 24.5 mol % Na_2O, and 6 mol % P_2O_5.[9] The 45S5 glass composition offers remarkable advantages, owing to its high bioactivity and osteoconductivity. During the dissolution of this BG, its main ions (calcium, silica,

Received: May 24, 2024
Revised: November 24, 2024
Accepted: December 9, 2024
Published: December 24, 2024

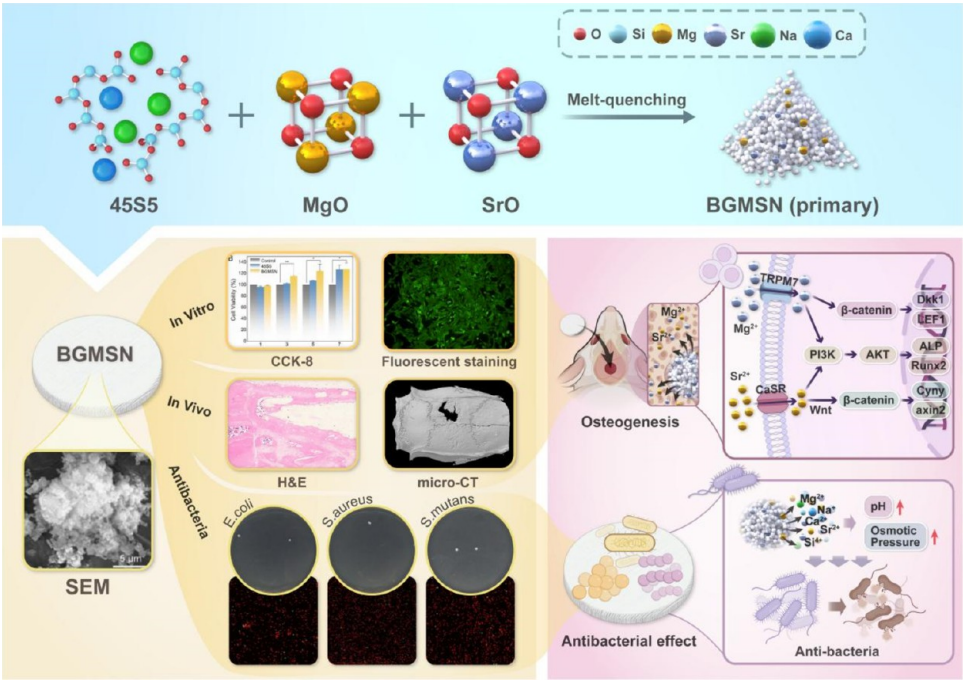

Figure 1. Synthesis method of novel bioactive glass BGMSN, its experimental results *in vitro* and *in vivo*, and the potential-related mechanisms.

sodium, and phosphate) are released; then, they combine with the ions from the environment to form a carbonated hydroxyapatite (CHA) bone-like mineral coating. Finally, the CHA layer establishes strong bonds with the surrounding bone, encouraging and stimulating its growth. In addition, many studies on 45S5 bioglass, both *in vitro* and *in vivo*, have shown that this glass can be used to produce scaffolds (at a tailored porosity exceeding 90%) for tissue engineering.[10]

In addition, several recent studies have demonstrated the modification of BGs using different elements or components to confer additional functions.[11] For instance, magnesium forms the basis of bone metabolism and promotes osteoblast differentiation, proliferation, and mineralization,[12] in addition to being among the most significant ions associated with biological apatite. Accordingly, some studies have incorporated Mg into bone-interfacing biomaterials and reported its beneficial properties. The addition of Mg ions to a bioactive porous scaffold has been shown to lead to new bone formation.[13] This was attributed to Mg ions enhancing BMSC proliferation, migration, osteogenic differentiation, and angiogenesis via mitogen-activated protein kinase/extracellular signal-regulated kinase pathway activation. For instance, Mg^{2+} can elevate the expression of runt-related transcription factor 2 (Runx2) and alkaline phosphatase (ALP) via the TRPM7/PI3K signaling pathway, thereby strengthening the osteogenic activity of osteoblasts.[14] Recently, Zhou et al.[15] reported that the addition of Mg^{2+} can activate the canonical Wnt signaling pathway, leading to a substantial upregulation in the expression of β-catenin and its downstream genes, such as LEF1 and DKK1. This triggers the differentiation of human bone marrow stromal cells (hBMSCs) into the osteoblast lineage, inducing an osteogenic effect. Strontium has also been shown to enhance the osteoinductivity of different bone implants, including titanium alloys, BGs, and ceramics.[16] Actually, Sr is a bone-tracking trace element with dual effects on bone metabolism, it promotes the proliferation and differentiation of osteoprogenitor cells but inhibits the terminal differentiation of osteoclasts.[17] Levels of key genes associated with the Wnt/β-catenin pathway, specifically axin-2 and c-myc, have been observed to be elevated in BMSCs that were treated with 6% Sr-MSNs.[18] Furthermore, some studies have indicated that Sr promotes an improved antibacterial efficiency.[19−21] Sr can be substituted into hydroxyapatite by replacing some calcium ions to obtain Sr-substituted calcium phosphates (Sr-CaPs), which have been reported to exhibit antimicrobial properties.[14] In addition, Sr- and Mg-doped hydroxyapatite (HAP) have demonstrated good antibacterial effects, which were attributed to bonding between the metal ions and the functional groups of proteins present on the bacterial cell membranes.[21] The resulting structural changes eventually lead to the death of the microorganisms. However, the antibacterial activities of such materials depend on many factors, such as the metal ion concentration, the structure of the bacterial cell membrane, and pH variation. Therefore, it is necessary to investigate the osteogenic and antibacterial activities of BGs that incorporate Sr and Mg in the context of the repair and functional reconstruction of bone defects. Moreover, the results show that the Sr−Mg codoped calcium phosphate scaffold has higher biocompatibility than the simple scaffold.[22,23] *In vivo* studies have shown that HAP codoped with Sr−Mg can promote osteoblast proliferation and new bone formation.[24] The combined action of Sr^{2+} and Mg^{2+} can produce a synergistic effect of PI3K/Akt pathway activation, improve the osteogenic ability, and further promote osteogenesis and angiogenesis.[25] These all show the advantages of Sr−Mg codoping.

In this study, a fusion-quenching method was used to create a novel antibacterial BG material for bone regeneration. For this purpose, SrO and MgO were added to BG during sintering to prepare a novel bioactive glass doped with Mg−Sr (BGMSN). To determine the suitability of the prepared BGMSN for use in bone tissue engineering applications, initial *in vitro* bioactivity investigations were carried out to verify that this material generated hydroxyapatite crystals when immersed

https://doi.org/10.1021/acsomega.4c04898
ACS Omega 2025, 10, 215−229

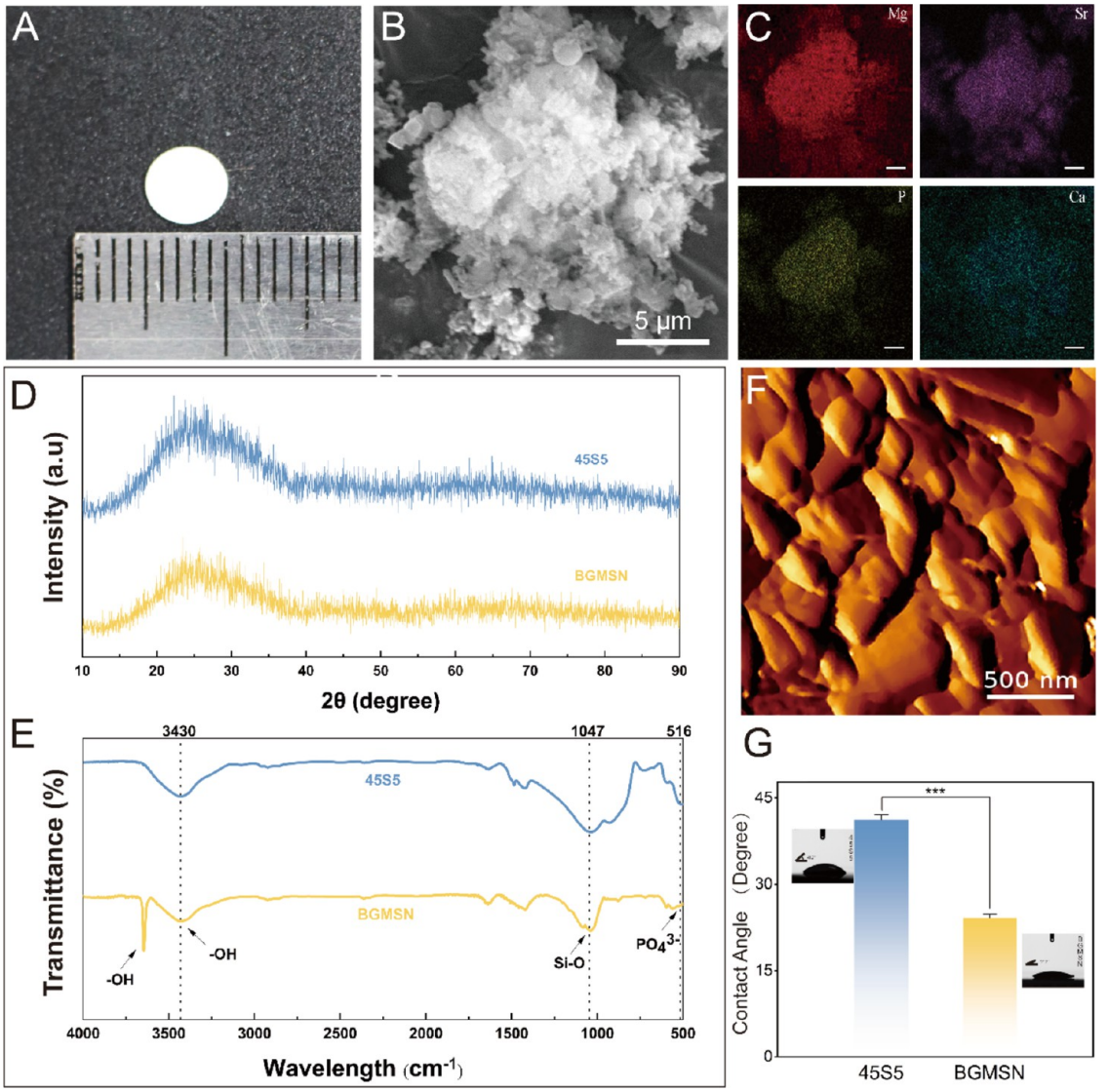

Figure 2. Characterization of the BGMSN. (A) Photograph of BGMSN. (B) SEM microscopy images of the BGMSN. (C) EDS mappings of BGMSN. (D) XRD patterns of BGMSN and 45S5. (E) FTIR spectra of BGMSN and 45S5. (F) AFM images of BGMSN. (G) Water contact angle degree of BGMSN and 45S5 and quantitative analysis (***$P < 0.001$).

in simulated body fluid (SBF). In addition, the biocompatibility, osteogenic induction, and antibacterial properties of BGMSN were assessed both *in vitro* and *in vivo* using a battery of experiments. The possible osteogenic and antibacterial mechanisms are described in Figure 1. We hope that this novel BGMSN will offer an alternative treatment for bone defects, including bone infections.

2. RESULTS AND DISCUSSION

2.1. Characterization of the BGMSN. *2.1.1. Physicochemical Structure of the BGMSN.* Figure 2 shows the physicochemical structures and properties of the prepared BGMSN and 45S5 BG. From the BGMSN morphology shown in Figure 2A, it can be observed that this material was uniformly round with a slightly rough surface. In addition, the BGMSN consisted of a large number of micrometer-sized particles with heterogeneous sizes, as shown via scanning electron microscopy (SEM) at different magnifications (Figures 2B and S1). Energy-dispersive spectroscopy (EDS) mapping showed that P, Ca, Mg, and Sr were present on the surfaces of the BGMSN (Figure 2C), thereby confirming the successful introduction of Sr and Mg ions into the Si-based BG by melt quenching. As shown in Figure 2D, the analysis of the X-ray diffraction (XRD) pattern confirmed the amorphous structure of the BGMSN. At a 2θ value of approximately 23°, a wide peak characteristic of silicate glass can be observed. This indicates that BGMSN maintained good stability at the given sintering temperature. The functional groups present in 45S5 and BGMSN were determined using Fourier transform infrared (FTIR) spectroscopy (Figure 2E). More specifically, peaks corresponding to the phosphate and hydroxyl groups of both materials were observed at 516 and 3430 cm^{-1}, respectively, whereas a peak corresponding to the Si−O bonds of 45S5 and BGMSN was present at approximately 1047 cm^{-1}. In addition, an additional hydroxide peak was observed for the BGMSN specimen at approximately 3644 cm^{-1}, which was attributed to the addition of the oxides. As shown in the atomic force microscopy (AFM) images in Figure 2F, the surface morphology of BGMSNs was rougher than that of 45S5 (Figure S2), which is conducive to cell adhesion.[26]

https://doi.org/10.1021/acsomega.4c04898
ACS Omega 2025, 10, 215−229

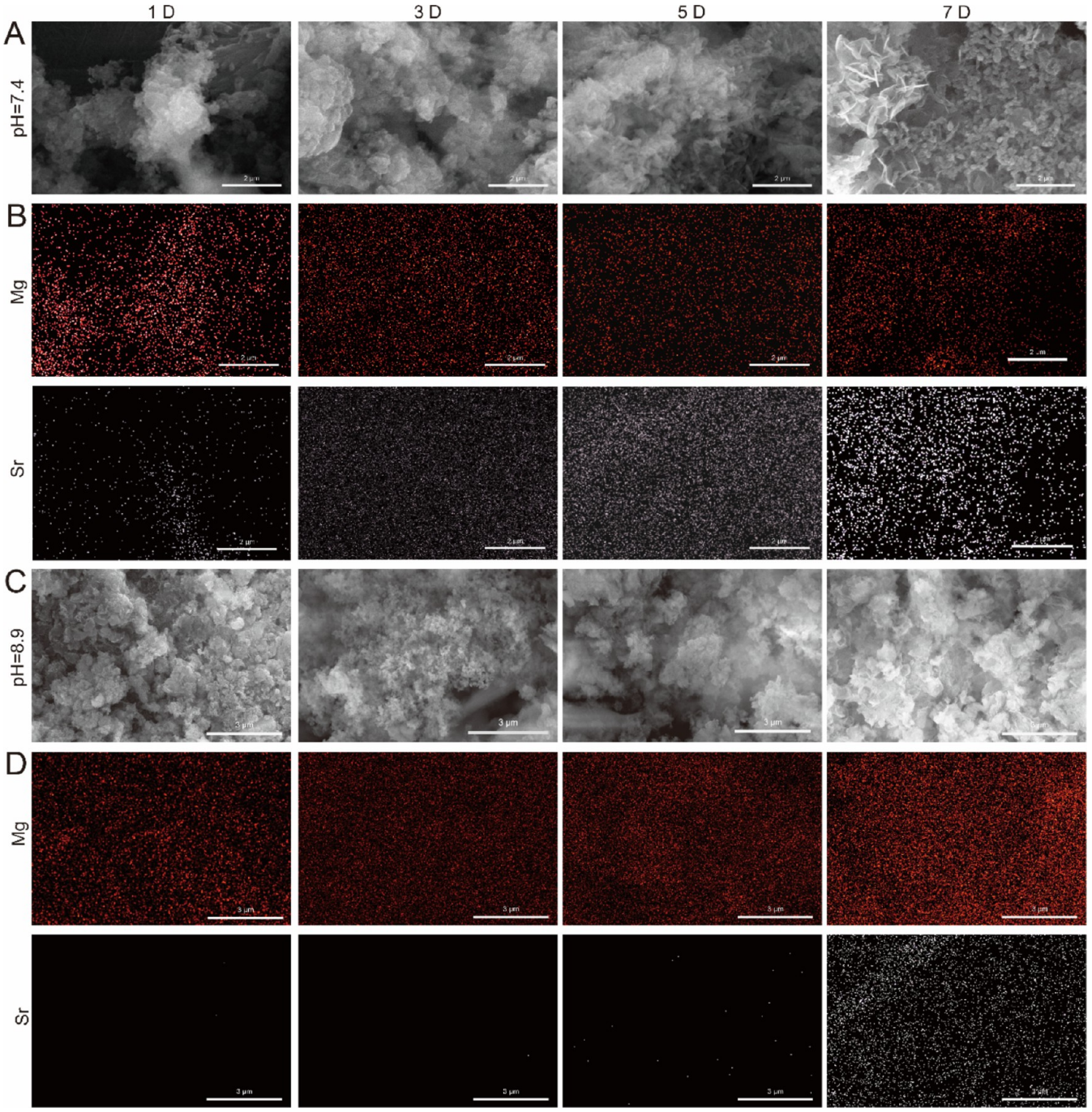

Figure 3. Mineralization of BGMSN in SBF at Different pH Values. (A) SEM microscopy images of BGMSN after immersion in SBF at pH 7.4 for 1, 3, 5, and 7 days, respectively. (B) EDS spectra of BGMSN after immersion in SBF at pH 7.4. (C) SEM microscopy images of BGMSN after immersion in SBF at pH 8.9, for 1, 3, 5, and 7 days, respectively. (D) EDS spectra of BGMSN after immersion in SBF at pH 8.9.

Furthermore, the water contact angles determined for the BGMSN and 45S5 specimens were 23.7 ± 1.6° and 40.7 ± 1.4°, respectively, indicating their hydrophilic nature. Notably, BGMSN were more hydrophilic than 45S5 BG ($P < 0.001$), providing favorable conditions for osteogenesis (Figure 2G). Moreover, studies have confirmed that materials with higher surface free energy are more conducive to cell adhesion.[6] In order to reasonably infer the interaction between BGMSN surface and cells, the Owens and Wendt geometric average method based on contact angle was used to quantitatively calculate the surface free energy of different bioactive glass samples.[27] As shown in Figure S4, compared with the surface of 45S5 (55.9 mJ/m^2), the surface of BGMSN (66.6 mJ/m^2) had stronger hydrophilicity and increased surface free energy.[28] Besides, BGMSN's surface exhibited a significantly higher ($P < 0.001$) polar component of surface free energy (47.9 mJ/m^2) compared to 45S5's surface (38.5 mJ/m^2). Additionally, the dispersion components of surface free energy for BGMSN and 45S5 were 18.71 and 17.3 mJ/m^2, respectively ($P < 0.05$). The results indicated that the introduction of Sr and Mg could improve the hydrophilicity of the bioactive glass surface, which was conducive to cell adhesion. In general, it can be inferred that the BG surface with the introduced Sr and Mg elements is a cell-friendly surface. Appropriate wettability and high surface

https://doi.org/10.1021/acsomega.4c04898
ACS Omega 2025, 10, 215−229

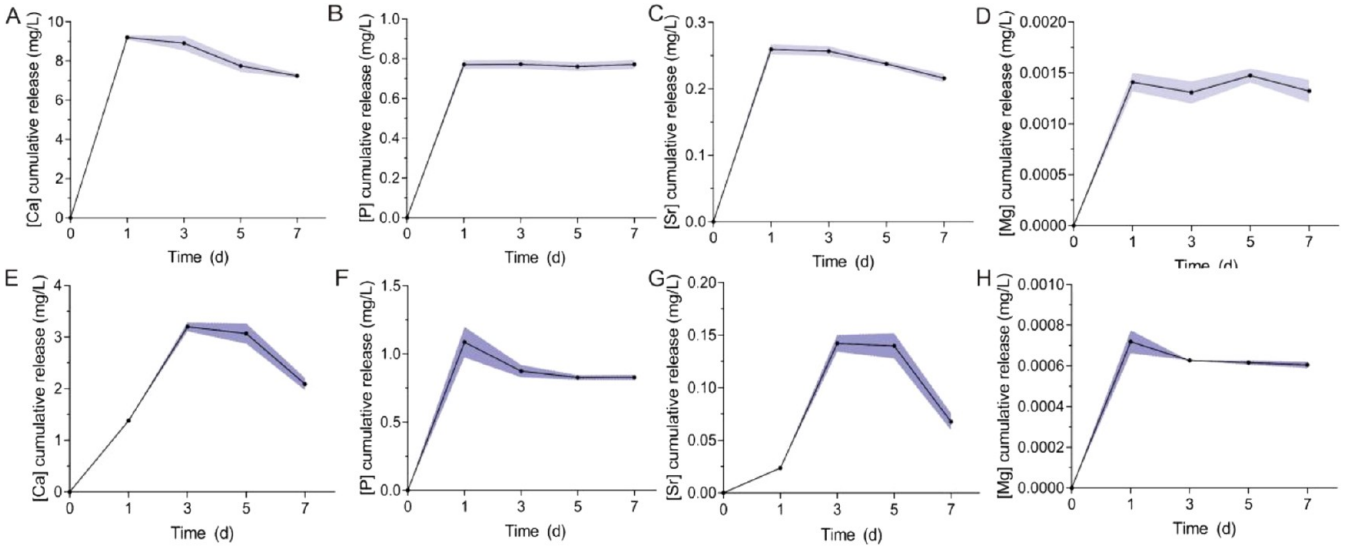

Figure 4. ICP-AES measured the evolution of the Ca ion (A, E), P ion (B, F), Sr ion (C, G), and Mg ion (D, H) of the BGMSN immersed in SBF of pH 7.4 (A–D) and pH 8.9 (E–H), respectively, up to 1, 3, 5, and 7 days.

free energy promote cell adhesion, migration, and proliferation.[29]

It should be noted that a glass composite can be sintered without crystallization, whereas the remaining bioactive material is extremely challenging. It is true that full crystallization reduces bioactivity, whereas partial crystallization leads to instability caused by preferential degradation of the residual amorphous regions.[30] After adding Sr and Mg ions, the prepared BGMSN still exhibited a stable noncrystalline structure with an increased roughness and hydrophilicity.

2.1.2. Apatite-Forming Ability of the BGMSN. The biological activity of glass is an important indicator of its potential for application in biological systems. Thus, the ion release and mineralization properties of the prepared BGMSN were analyzed according to the standardized Kokubo protocols.[31] Figure 3A outlines the *in vitro* mineralization properties of the BGMSN in SBF. More specifically, the BGMSN were incubated in SBF for 1, 3, 5, and 7 days prior to analysis using SEM and EDS. As shown in Figure S5, after 3 days, some cauliflower-like hydroxyapatite (HA) deposits formed on the BGMSN surfaces, whereas after 5 days, the surface was almost completely covered with HA sediment. In addition, after 7 days of incubation, a mineralized globule was formed on the BGMSN, as confirmed by EDS, wherein HA with a Ca/P ratio of approximately 1.5:1 was detected (Figures 3B and S6), which is close to the Ca/P ratio observed in human bone tissue (i.e., 1.49:1). Furthermore, the FTIR spectrum was measured after 7 days of incubation (Figure S7), and characteristic peaks corresponding to HA were observed at 566 and 604 cm^{-1}, which were attributed to the presence of PO_4^{3-}. Moreover, the characteristic peaks at 1635 and 473 cm^{-1} are attributed to −OH bending vibrations and the presence of the O−Si−O bonds, respectively. These data confirmed the successful formation of HA on the BGMSN surfaces. Notably, this HA layer has the ability to rapidly generate a strong bond between the BG and bone tissue to enhance osseointegration, thereby suggesting that the prepared BGMSN may exhibit good osteogenic properties.

The ionic profiles of the BGMSN were determined via ICP-AES for Ca, P, Sr, and Mg by analyzing the SBF solutions from 1, 3, 5, and 7 days. The mineralization process of BGs immersed in SBF involves a complex mechanism of ion exchange between surface and medium.[32] As the silica network starts to degrade, active cations such as Ca^{2+}, Mg^{2+}, and Sr^{2+} but also anions such as SiO_4^{4-} and PO_4^{3-} (and their protonated forms) are released in the medium. Then, with the SBF solution being supersaturated regarding the hydroxyapatite phase, Ca^{2+} and orthophosphate ions (PO_4^{3-}) reprecipitate on the bioglass surface and recombine to form amorphous and/or (poorly) crystalline calcium phosphates. As the apatite continues to deposit and crystallize on the BG surface, the diffusion of $PO_4^{3-}$and Ca^{2+} starts to decrease. At the same time, the release kinetics showed that BGMSN exhibited an early burst release of Sr and Mg ions during the first 24 h (Figure 4), followed by a slower diffusion-mediated release in the ranges of 7−9 and 0.0008−0.001 mg/L, respectively. The Sr^{2+} available in the solution was gradually consumed over time. This is because the lowering of Sr in the medium is the result of the difficulty in diffusing through these new phases/layers. The concentrations of Sr and Mg released in SBF were calculated to be 17.5 and 5.75 μg/g, respectively, which are in a biosafe range.

The ability to form apatite deposits under physiological conditions is necessary to initiate the bone regeneration process and is therefore a prerequisite for any material that may be considered to exhibit bone regeneration potential. The active apatite layer formed during the reaction between BG and physiological fluids is similar to the inorganic phase of bone, providing an adhesive interface with the tissue and acting as a scaffold to promote strong bonding with the bone. This is particularly desirable as it can prevent implant loosening. Therefore, the results of this *in vitro* biomineralization study suggest that the prepared BGMSN exhibit excellent apatite-forming ability, thereby rendering them possible for application in bone tissue repair and regeneration.

2.1.3. Mineralization of the BGMSN in SBF under Different pH Conditions. Owing to the proliferation of bacterial colonies in chronic wounds, these areas possess pH values ranging from 7.3 to 10.[33] More specifically, chronic wounds often exhibit a spatial irregularity of infection development owing to their nonuniform healing rate, resulting in drastic pH variations throughout the affected area, the pH

https://doi.org/10.1021/acsomega.4c04898
ACS Omega 2025, 10, 215−229

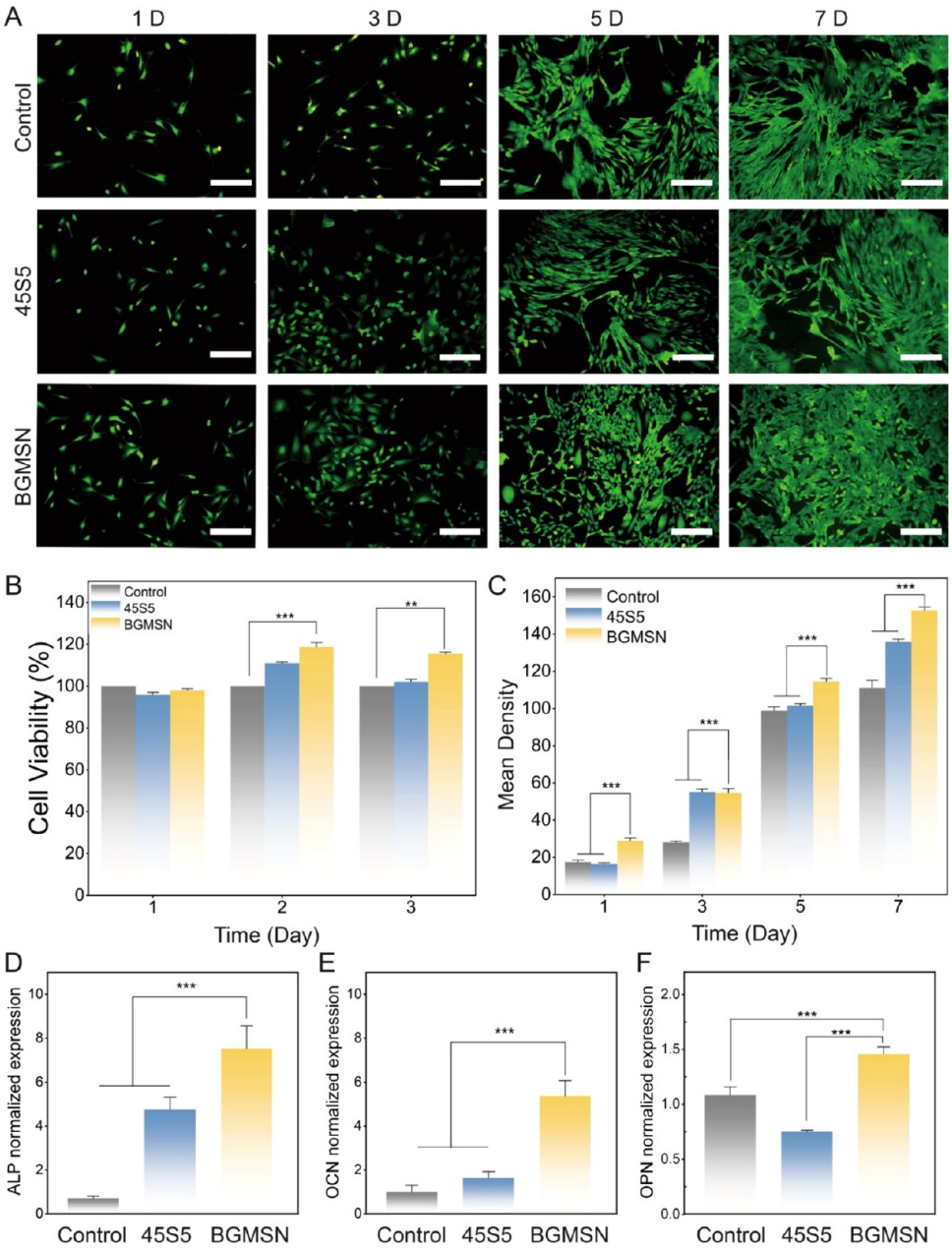

Figure 5. *In vitro* biological activity of BGMSN. (A) Calcein fluorescent staining of MC3T3-E1 after cocultured with BGMSN and 45S5 for 1, 3, 5, and 7 days (scale bars = 200 μm). (B) Proliferation of L-929 cells cultured with liquid extracts of BGMSN or 45S5 by CCK8 assay for 1, 2, and 3 days (*P < 0.05, **P < 0.01). (C) Quantitative analysis of calcein fluorescent staining (***P < 0.001). (D−F) ALP, OCN, and OPN expressions of MC3T3-E1 under BGMSN and 45S5 treatments were determined by ELISA (**P < 0.01,***P < 0.001).

value of the wound surface is commonly between 7.5 and 8.9.[34−36] Therefore, we chose SBF with a pH 8.9 to try to simulate the alkaline environment of chronic wounds to verify whether BGMSN can play a role in this situation and deposition of hydroxyapatite to promote osteogenesis. As shown in Figure 3C, after 1 day of immersion in SBF at pH 8.9, the BGMSN surfaces were almost completely covered with plate-like HA nanocrystals. After 3 days, both pH 7.4 (Figure 3A) and 8.9 (Figure 3C) conditions led to the formation of an HA layer on the BGMSN surfaces, with this layer being slightly denser for the pH 8.9 conditions. After immersion for 5 and 7 days, crystal deposition continued under both pH conditions to gradually generate plate-like structures, although the lamellar structure obtained at pH 7.4 appeared to be looser. The results indicated that a HA layer was formed on the BGMSN surface when the pH was 8.9. Furthermore, the EDS results reveal that for BGMSN immersed in SBF with pH 8.9 (Figure 3D), the deposition of Mg ions commenced on the 1st day and gradually increased over time. Sr ions deposited on the glass surface of the BGMSN immersed in SBF with pH 8.9 (Figure 3D) were also gradually increased over time. As shown in Figure S9, there was significant deposition of Ca and P ions regardless of the pH environment. Moreover, the FTIR spectra (Figure S8) generally matched those of HA. More specifically, an O−H stretching band was observed at 1635 cm^{-1}, and peaks corresponding to PO_4^{3-} were observed at 566 and 604 cm^{-1}. Notably, after the 1st day, an additional peak was observed in the samples at 1500 cm^{-1}, which was attributed to

https://doi.org/10.1021/acsomega.4c04898
ACS Omega 2025, 10, 215−229

the CO_3^{2-}. The presence of this peak suggests the incorporation of carbonate ions (from ambient CO_2) into the biomimetic apatite to generate carbonate-HA ($Ca_{10}(PO_4)_3(CO_3)_3(OH)_2$).[24]

The ion release results showed that (Figure 4E−H), on the 1st day, calcium was still in the accumulation and release stage in PBS (pH 8.9), and on the 3rd day, the hydroxyapatite phase reached supersaturation and was deposited on the surface of BGMSN, showing a gradually decreasing trend. However, overall, the concentration of calcium decreased compared to that of SBF (pH 7.4) in the range of 1.3−3 mg/L. The Sr concentration was relatively low, ranging from 0.02 to 0.14 mg/L. More precisely, the ion release was in a stage of slow rise for the first 3 days and then continued to decrease after reaching equilibrium on the 5th day. This indicates that BGMSN rapidly produced mineral deposits after contact with SBF and consumed Ca and Sr elements in the SBF solution.[37] The Mg ion concentration decreased significantly on the 3rd day of mineralization and then remained stable, with a concentration in the range of 0.00006−0.0007 mg/L. The P release trend in SBF at both pH levels was similar and remained in the stable range of 0.8−1 mg/L after the 1st day.

In clinical practice, the generation of bone defects from tumors, infections, or other bone diseases remains an ongoing challenge. The pathological microenvironments of these bone defects can further affect bone regeneration.[1] Indeed, both internal and external stimuli can alter the internal atomic packing arrangements of materials, which can impact cell viability and consequently enhance bone tissue therapy and regeneration. For example, excess reactive oxygen species and mildly acidic conditions are commonly found in the tumor microenvironment, whereas severe bacterial infections can lead to characteristic pH levels and enzyme secretion. Biochemical triggers can be used at bone defect sites to activate bone regeneration.[1] Notably, at pH levels associated with infected wounds, the prepared BGMSN was found to rapidly deposit HA, with visually detectable levels present on the 3rd day. This may be partly because of the presence of Sr ions, because Sr can significantly enhance apatite formation. It has been hypothesized that Sr^{2+} may potentially enhance the precipitation of apatite by facilitating the formation of a higher number of nucleation clusters.[38] These results demonstrate that under the specific environmental conditions of severe wound infection, BGMSN can deposit HA to promote bone formation, thereby allowing the pH to act as a biochemical trigger for BGMSN to activate bone disease treatment and bone regeneration.

2.2. *In Vitro* Cell Biocompatibility, Induction of Osteogenic Differentiation, and Antimicrobial Properties of the BGMSN. *2.2.1. In Vitro Cell Biocompatibility of the BGMSN Material.* To verify the biocompatibility of the prepared BGMSN, the *in vitro* biological activity of this material was evaluated, as outlined in Figure 5. L-929 cells, MC3T3-E1 cells, and Human Gingival Fibroblast (HGF-1) cells were cultured with the extracted liquid BGMSN and 45S5 to evaluate the biocompatibility of the material. As shown in Figure 5B, after 1 day of culture, similar cell viabilities were obtained for the BGMSN-treated, 45S5-treated, and control groups, indicating that the cells were in a normal growth state. Similar results were obtained after 2 and 3 days of culture, with no cytotoxicity detected. However, the BGMSN group exhibited a significantly superior proliferative effect ($P < 0.05$). Specifically, the cell viabilities of the BGMSN group on the 2nd and 3rd days were 118 and 115%, respectively. To prove that BGMSN has no cell specificity, HGF-1 cells were also cultured with the liquid extract. As shown in Figure S10, after 1 and 3 days of culture, similar cell viabilities were obtained for the BGMSN-treated and control groups, indicating that the cells were in a normal growth state. However, the BGMSN group exhibited a superior proliferative effect after 5 and 7 days of culture, and this difference was statistically significant ($P < 0.05$). Specifically, the cell viabilities of the BGMSN group on the 5th, and 7th days were 117 and 128%, respectively. This demonstrates the good biocompatibility of BGMSN. The proliferative effects of BGMSN were subsequently investigated in detail, and calcein fluorescence staining was used to assess the differences in cell proliferation and adhesion. As shown in Figure 5A, the cell densities of the BGMSN and 45S5 treatment groups were similar to those of the control group on the 1st day, and the majority of cells appeared to be fibroblast-like. The total number of BGMSN cells on the 3rd, 5th, and 7th days significantly increased, and there was a statistically significant difference between all groups after the 5th day. Moreover, as shown in Figure 5C, BGMSN treatment led to a greater degree of proliferation after 1 day ($P < 0.001$). These results were consistent with those of the cell viability experiments, indicating that the BGMSN exhibited superior biocompatibility.

In general, the regeneration of large bone defects necessitates the utilization of biomaterials to bridge tissue gaps and provide structural support, thereby maintaining physiological activities and facilitating cellular behaviors, such as nutrient transport, cell adhesion, proliferation, migration, differentiation, and maturation, during new bone formation. Therefore, the results support the potential application of prepared BGMSN *in vivo*.

Compared with BG doped with magnesium alone, BG with a Sr/Mg mole ratio of 1/2 did not have more desirable cell-biological performances in promoting osteogenesis and inhibiting osteoclastic activities.[38] Some scholars have prepared Mg/Sr phosphate bioceramics with Sr/Mg mole ratios in a narrower range of 0−0.5. The bioactivity was not significantly different.[39] This may be because of the various factors affecting the cell response; none of the bioceramics showed the most desirable cell behavior in every cell activity. In this study, novel BGs doped with Mg/Sr with a Sr/Mg mole ratio of 2/1 were prepared. Showing the achievement of good biocompatibility, combined with previous studies and our experimental data, it is proved that when the Sr:Mg molar ratio is 2/1, the improved BG may be applicable in the future treatment of bone defects.

2.2.2. Effects of the BGMSN on Osteogenic Differentiation. Bone formation involves a combination of multiple molecules and proteins, including osteocalcin (OCN), ALP, and osteopontin (OPN). These molecules are involved in bone mineralization and calcium metabolism, which are crucial for bone formation. More specifically, OCN regulates calcium metabolism during bone formation, and to a certain extent, OCN represents osteoblast maturation.[40] ALP is an enzyme secreted by osteoblasts and a marker for early osteoblast differentiation and represents osteoblast maturation. Several studies have shown that ALP affects the process of bone mineralization by participating in the deposition process of HA.[41] Meanwhile, OPN is a negatively charged non-collagenous bone matrix glycoprotein with mineralizing properties; it contains acidic domains that can interact with

https://doi.org/10.1021/acsomega.4c04898
ACS Omega 2025, 10, 215−229

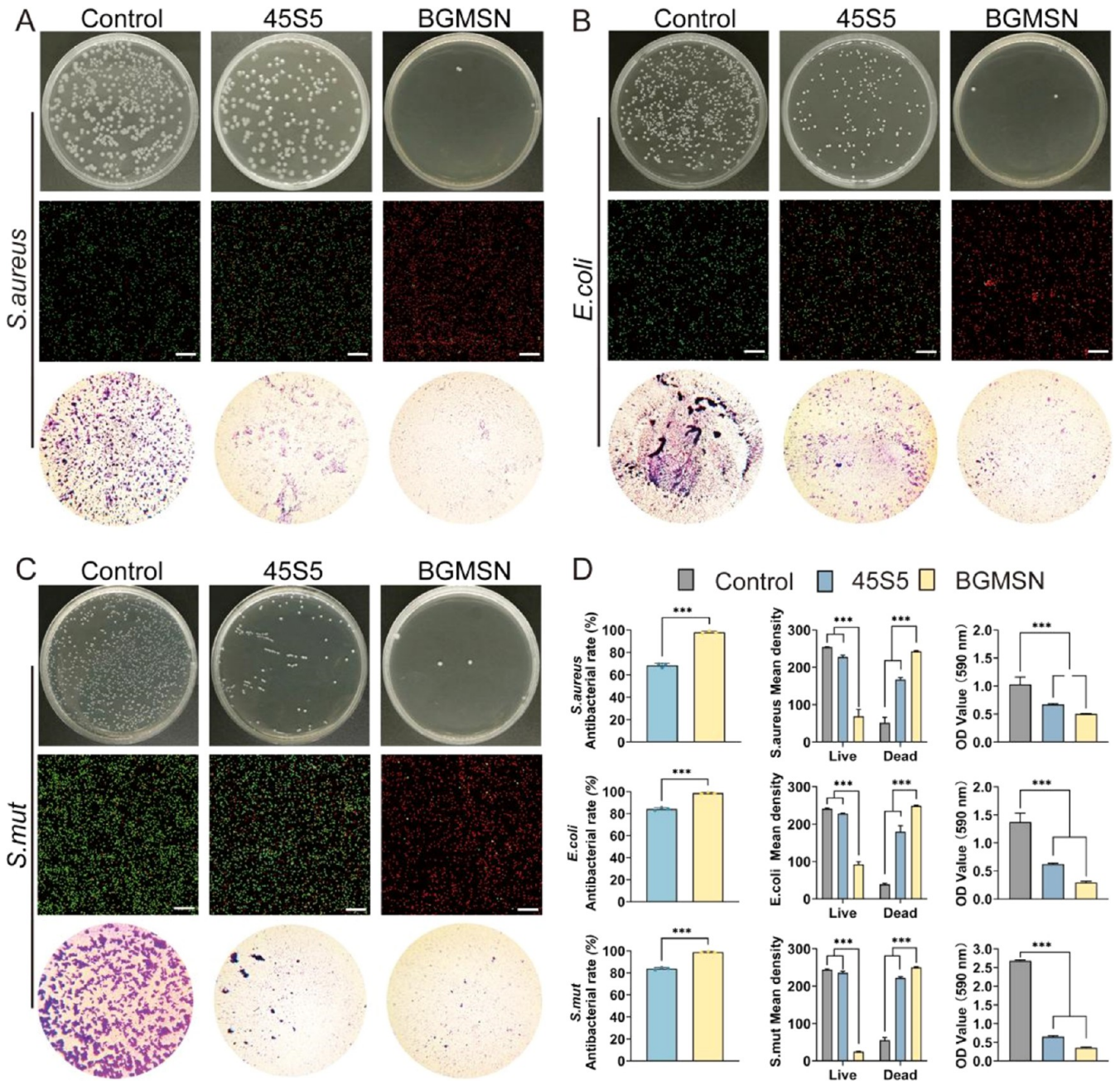

Figure 6. Antibacterial activities of BGMSN and 45S5. (A−C) Photographs of colony plate counts and live/dead staining of bacteria attached to the surface after coculturing BGMSN and 45S5 bioactive glass with *S. aureus*, *E. coli*, and *S. mutans* for 6 h, as well as biofilm growth. (D) Quantitative analysis of the bacteriostatic rate, live/dead staining fluorescence intensity, and crystal violet staining of biofilm of *S. aureus*, *E. coli*, and *S. mutans* (***$P < 0.001$), (scale bars = 20 μm).

the mineral surface of the extracellular matrix and is closely related to bone formation and development.[42] As shown in Figure 5D−F, after coculturing MC3T3-E1 cells with the 45S5 and BGMSN leaching solutions for 7 days, the expression of osteogenesis-related genes was upregulated in both groups, although the BGMSN group demonstrated significant upregulation ($P < 0.001$). ALP, a typical marker of early osteoblast formation, affects bone mineralization by participating in HA deposition. In contrast, OCN is an important indicator of osteoblast maturation, as it is a product of late-stage osteoblast differentiation. Compared to the 45S5 group, BGMSN treatment significantly upregulated both ALP and OCN expression (Figure 5D,E) ($P < 0.001$), indicating that BG may activate the proliferation and differentiation of osteoblasts more effectively, thereby promoting osteogenesis. In addition, BGMSN significantly upregulated the level of the expression of the OPN (Figure 5F), whereas the regulatory effect of 45S5 on the level of the OPN was relatively limited. This suggests that BGMSN plays a more active role in bone mineralization than 45S5 BG does.

We think that the superior biological activity of BGMSN is attributable to the presence of Sr and Mg. Studies have shown that Sr^{2+} enhances the expression of osteoblast-related genes, exhibits nontoxic properties to cells even at elevated concentrations, enhances the capacity for apatite development by reducing the time required for its formation, and facilitates

https://doi.org/10.1021/acsomega.4c04898
ACS Omega 2025, 10, 215−229

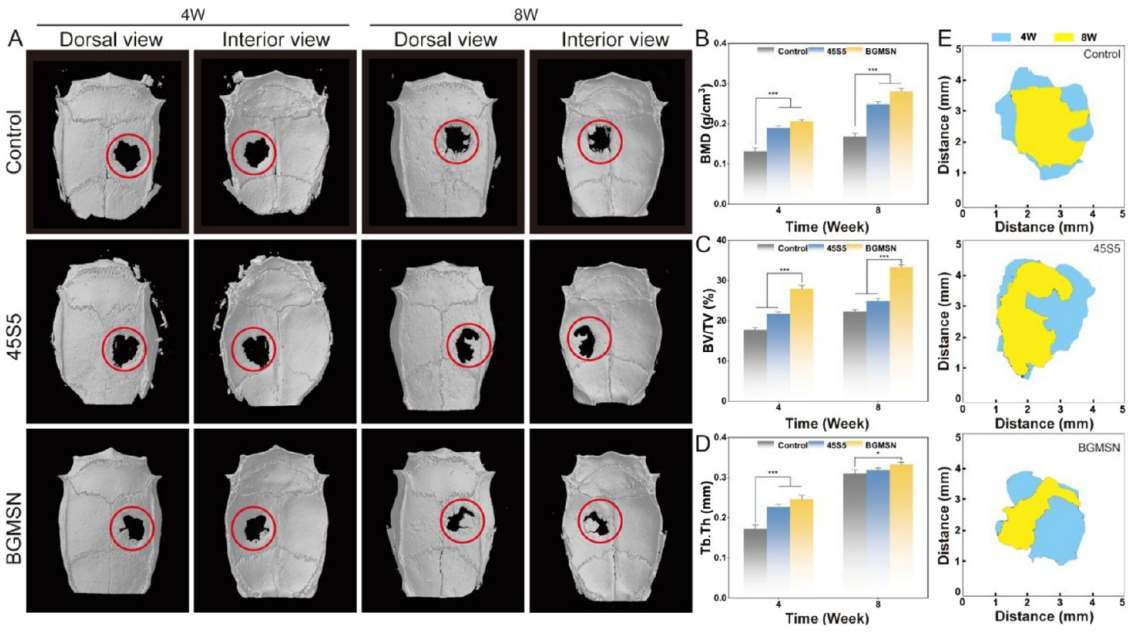

Figure 7. Osteogenic evaluation of BGMSN *in vivo*. (A) Three-dimensional reconstruction of 4- and 8-week calvarian specimens of the control, 45S5, and BGMSN groups. (B) Bone mineral density (BMD) measurements of the three groups (***$P < 0.001$). (C) Bone score values (BV/TV %) measurements of the three groups (***$P < 0.001$). (D) Trabecular thickness measurements of the three groups (*$P < 0.05$). (E) Bone mass model diagram of the three groups.

bone densification.[43] Detailed *in vitro* studies have confirmed the ability of Mg ions to stimulate osteoblast differentiation and inhibit osteoclast formation in a dose-dependent manner.[44] Furthermore, it should be noted that the component ions of BG (i.e., Ca, Si, and P) are crucial in the process of bone regeneration. More specifically, Ca is an important component of the mineralized bone matrix and can induce the proliferation of mesenchymal progenitor cells and mature osteocytes,[45] its role in bone tissue repair is well recognized. In addition, Si can reduce bone absorption caused by Ca deficiency while also increasing bone density,[46] inducing the production of collagen I in human osteoblasts, promoting osteoblast differentiation.[47] Moreover, P participates in various physiological processes and regulating the differentiation and mineralization of osteoblasts and preosteoblasts.[48]

2.2.3. In Vitro Antimicrobial Activity of the BGMSN. Clinically, the occurrence of an infection around an implant frequently results in severe consequences, often necessitating surgical debridement for implant removal. Amputation and disability may occur in extreme cases. Therefore, the development of implant materials with antibacterial properties is extremely desirable. *S. aureus* is a frequent colonizer of the human population and is one of the most opportunistic bacterial pathogens in humans.[49] As such, it was selected as a representative Gram-positive bacterium to evaluate the antibacterial activities of the BGMSN and 45S5 materials. *Escherichia coli* is a leading pathogen that induces harmful implant-associated infections in surgical patients; therefore, it was selected as a representative Gram-negative bacterium.[50] Similarly, *Streptococcus mutans* has a strong affinity for tooth surfaces and tissues. Consequently, to ensure the success of intraoral implants, suppression of the attachment of *S. mutans* to implant surfaces after surgery is crucial for enhancing osseointegration. This also represents a facultative anaerobe.[51] Figure 6 demonstrates the excellent antimicrobial properties of the prepared BGMSN, wherein the measurement of the colony-forming units (CFU) indicated that the broad-spectrum bacteriostatic rate of BGMSN was >90% ($P < 0.001$), thereby highlighting their prominent antibacterial properties compared to the 45S5 and blank control groups. Specifically, the antibacterial rates against *E. coli* in the BGMSN group reached up to 98.7%, while the antibacterial rate of *S. aureus* was 98%, and the antibacterial rate of *S. mutans* was 98.8%. These values were significantly higher than those in the 45S5 group (84.4, 68.5, and 83.9%, respectively). These results were further confirmed by confocal fluorescence microscopy, wherein a greater number of red-stained areas were observed in the BGMSN group, corresponding to dead bacteria. More specifically, the live/dead ratios of the three groups are presented in Figure 6, wherein it is apparent that the live/dead ratio obtained for the 45S5 group was significantly higher than that for the BGMSN group ($P < 0.001$). In the control group, the bacterial growth was not effectively inhibited. Instead, a dense biofilm was formed, and the optical density (OD, 590 nm) was significantly higher than those of the 45S5 and BGMSN groups. The line chart in Figure S11 illustrates the trends of bacterial growth in the different study groups, showing that for the three pathogenic bacteria in the BGMSN group, the OD values gradually decreased and stabilized after 6 h. In contrast, the OD value of the 45S5 group increased slowly during the same period, indicating a statistically significant difference in the 6 h OD values between the BGMSN, 45S5, and control groups ($P < 0.001$). Therefore, these results indicate that the BGMSN exhibits superior antibacterial properties compared to 45S5 BG, which may be because of the enhanced antibacterial properties resulting from Sr and Mg doping. Considering that excellent antibacterial properties are a prerequisite for successful bone regeneration, these results suggest that BGMSN may exhibit excellent bone-induction capability.[20,21]

The antimicrobial mechanism of BG differs from that of conventional antibiotics. Specifically, the ionic lysates of BG

https://doi.org/10.1021/acsomega.4c04898
ACS Omega 2025, 10, 215−229

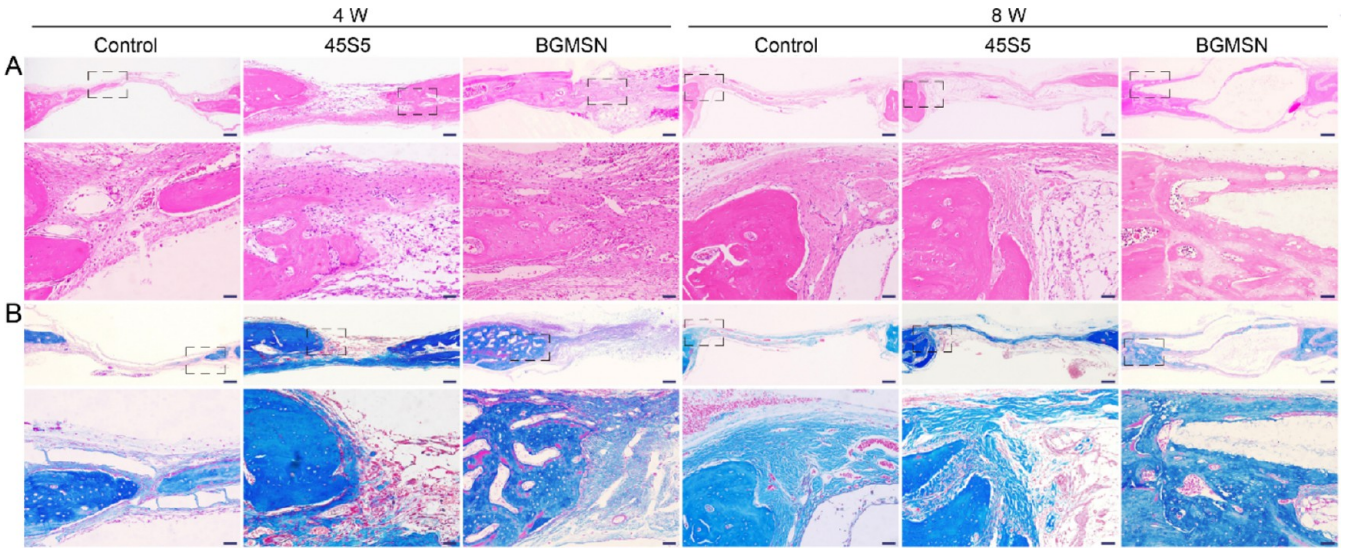

Figure 8. New bone regeneration assessment. (A) H&E staining images of the sections from calvarial defect model rats after 4 and 8 weeks of implantation of BGMSN. (B) Masson staining images (scale bars = 500 μm). The small image shows a representative image at 5× magnification (scale bars = 100 μm).

increased the pH and permeation of the medium, creating an unsuitable environment for bacterial proliferation. Contact between BG and biological fluids leads to the release of ions from particle surfaces, resulting in increased osmotic pressure and a higher pH, which renders the surrounding environment unfavorable for microbial growth.[19] Furthermore, according to a previous study,[52] BG doped with Sr demonstrated superior antibacterial effects compared to non-Sr-doped BG. The antibacterial mechanisms of Sr^{2+} may involve the inhibition of bacterial growth, cell wall synthesis, metabolism, and DNA replication. Further, the antibacterial effect on *S. mutans* may be due to the lack of silanization caused by the released Sr^{2+}.[53] However, the Sr-BG had low cytotoxicity (>70% viability) for particle concentrations of up to 250 μg/mL.[54] Ion release results of our study showed that the Sr concentration reached 268 μg/mL on the 1st day. Therefore, this is probably the maximum amount of Sr that can be incorporated while maintaining biological activity. Too little will affect its antibacterial effect on *S. mutans*, whereas too much will affect its biological activity. Notably, our study showed that BGMSN exhibits potent antimicrobial activity against both aerobic and anaerobic bacteria in their planktonic and fixed forms.

2.3. Osteogenic Evaluation of the BGMSN *In Vivo*.

2.3.1. 3D Reconstruction and Quantitative Statistics of Regeneration in a Rat Cranial Defect Area. Subsequently, the osteogenic effects of BGMSN were investigated *in vivo* to determine their role in promoting bone generation. More specifically, the prepared BGMSN and 45S5 BG were implanted into a rat calvarial defect model (Figure S12) and evaluated osteogenic after 4 and 8 weeks. The micro-CT results are shown in Figure 7A, the percentage of new bone area in the BGMSN, 45S5, and blank control groups was measured at each time point (4 and 8 weeks). The area of newly formed bone in the BGMSN group was greater than that in the other two groups, wherein new bone growth was initiated at the periphery of the defect and gradually progressed toward the center. At 8 weeks, the cranial defects in the BGMSN treatment group were almost completely covered by newly formed bone tissue. Bone mineral density (BMD) measurements revealed that the BGMSN group exhibited an average BMD of 0.28 g/cm^3, which was significantly higher than the 0.16 g/cm^3 observed in the blank control group at the 8 weeks (Figure 7B) ($P < 0.001$). Furthermore, the bone score values (BV/TV%) increased over time and were higher in the BGMSN group than in the other two groups at all examined time points (Figure 7C) ($P < 0.001$). Trabecular thickness (Tb.Th) in the BGMSN group is measured to be 0.33 mm at 8 weeks, which is higher than that in the other two groups (Figure 7D) ($P < 0.05$). As shown in the bone mass model diagram (Figure 7E), 4 weeks after implantation, the bone defect rate in the BGMSN group was 29.8%, which was significantly lower than that in the 45S5 group (46.3%). At the 8th week, the bone defect rate in the BGMSN group was only 17.3%, and new bone formation occurred at the edges of the BG; the highest amount of new bone tissue was detected in the BGMSN group.

2.3.2. Histological Assessment. The degree of new bone regeneration was assessed for each treatment group using hematoxylin and eosin (H&E) staining, Masson's trichrome staining, and immunohistochemical staining of the bone sections obtained from the calvarial defect model rats. Four weeks after implantation in the skull, H&E staining (Figure 8A) revealed a significant amount of new bone collagen fibrous connective tissue within the implant holes and surrounding the implant. New bone tissue was detected at the edges of the bone defect locations in both the BGMSN and the 45S5 groups. After 8 weeks, a greater number of red-stained areas were observed in the BGMSN group, indicating that this group exhibited a higher degree of collagen mineralization and bone maturity than the control and 45S5 groups. Masson's trichrome staining (Figure 8B) was used to observe the formation of collagen fibers and bone lacunae in the BGMSN and 45S5 groups, and the Masson's staining results corresponded with the quantitative micro-CT data. In particular, the BGMSN group showed the significant formation of a new bone matrix, indicating active bone integration into the defect area. This result was consistent with the trend observed in the *in vivo* bioactivity experiments, thereby confirming the positive effects on bone regeneration.

https://doi.org/10.1021/acsomega.4c04898
ACS Omega 2025, 10, 215−229

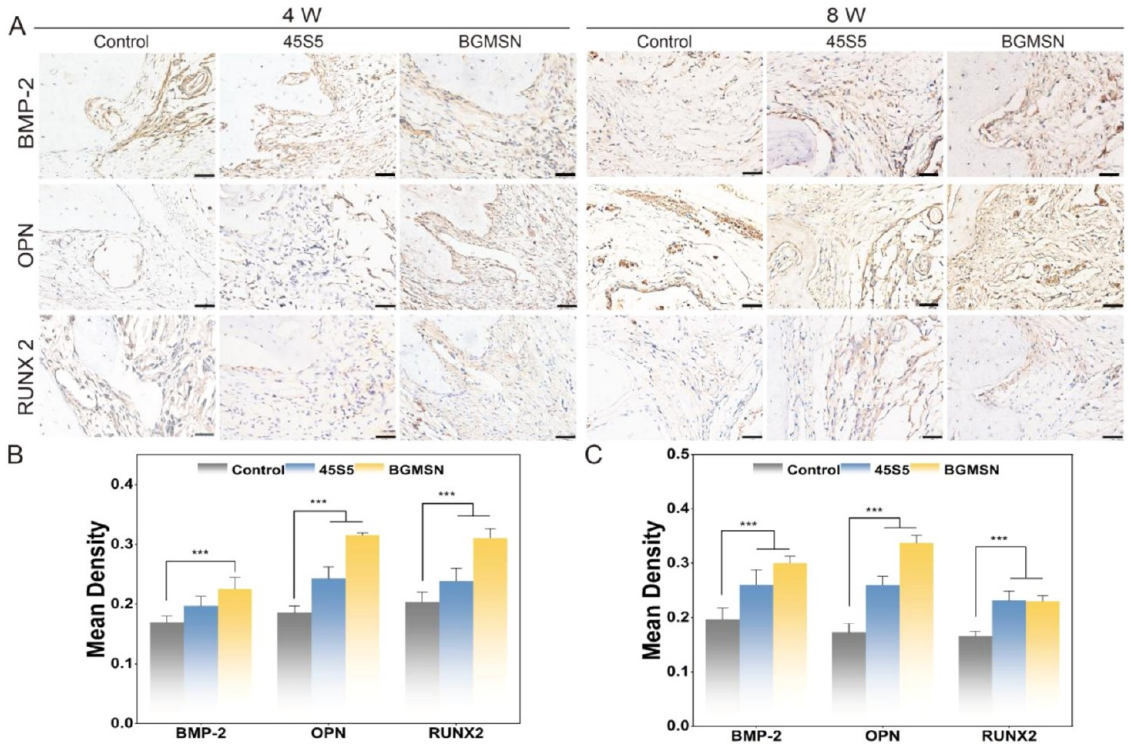

Figure 9. Expression of bone-related genes in newly formed bone. Using (A) BMP-2, RUNX-2, and OPN as markers to perform immunofluorescence staining on sections from calvarial defect model rats at 4 and 8 weeks (scale bars = 50 μm). (B) Quantitative analysis of positive staining area percentage of immunofluorescence staining of rats' skull defect model slices at 4 weeks (***$P < 0.001$). (C) Quantitative analysis at 8 weeks (***$P < 0.001$).

2.3.3. Immunohistochemical Fluorescence Staining Assessment. Bone morphogenetic protein-2 (BMP-2) is a multifunctional growth factor and an important marker of bone tissue growth, differentiation, and maturation.[55] In addition, OPN is an important indicator of late osteogenic differentiation.[42] During osteoblast differentiation, RUNX2 is weakly expressed in undifferentiated mesenchymal cells, upregulated in preosteoblasts, and reaches its maximum level in immature osteoblasts.[56] Thus, immunohistochemical staining and quantitative statistical analyses were used to evaluate the expression of osteogenesis-related proteins during bone repair after BG implantation *in vivo*. The brown-yellow and nuclear staining areas shown in Figure 9A represent the positive expression areas of BMP-2, the OPN, and RUNX2 at 4 and 8 weeks after implantation, respectively. It can be seen that 4 weeks after implantation, the expression levels of BMP-2, OPN, and RUNX2 in the BGMSN group were significantly higher than those in the control and 45S5 groups ($P < 0.001$). Furthermore, 8 weeks after implantation, the expression level of RUNX2 in the BGMSN group was significantly higher than that in the control group ($P < 0.001$), and there was no statistical difference between the 45S5 group. Moreover, the expression levels of BMP-2, OPN, and RUNX2 increased over time, with significantly higher levels detected in the BGMSN group than in the control group ($P < 0.001$). Additionally, quantitative analysis of the IHC images revealed that BMP-2, OPN, and OCN expression was more pronounced in the BGMSN group, and the difference between the groups was significant (Figure 9B,C; $P < 0.001$). These results indicated that BGMSN exhibited excellent osteogenic potential, which was consistent with the *in vitro* results. No evidence of organ damage was observed during the implantation period, indicating that the BG materials evaluated in this study did not cause systemic toxicity (Figure S13). BG promotes bone regeneration via a stepwise process that begins with calcium phosphate precipitation, followed by bone-like apatite formation on the surface and binding to hard tissues. The osteogenic performance of the prepared BGMSN, superior to that of the 45S5 BG, was attributed to doping with Sr and Mg ions. To some extent, Sr acts as an agonist of the calcium-sensing receptor (CaSR), which activates multiple intracellular signaling pathways to alter the cell behavior,[57] and to induce osteogenic viability, proliferation, and differentiation via the canonical Wnt signaling pathway, ultimately, this enhances bone formation.[18] For example, Sr^{2+} facilitates the differentiation and maturation of bone mesenchymal stem cells by enhancing the production of the downstream transcription factor RUNX2 via the Ras/MAPK signaling pathway.[14] Sr also promoted bone regeneration and osteogenesis through the activation of TGF-β/Smad and β-catenin signaling, as well as the upregulation of BMP-2 expression.[58] Furthermore, it prevents osteoclastogenesis by inhibiting the interaction between the rank ligand and its corresponding receptor, thereby playing a crucial role in bone metabolism.[59] It has also been reported that a lack of Mg affects all stages of skeletal metabolism, leading to decreased bone growth and lower osteoblastic activity. Research indicates that the activation of OPN through the CaM/CaMKIV/CREB1 signaling pathway is related to Mg^{2+}, and Mg ions can activate PI3K phosphorylation through the Mg ion transporter TRPM7, ultimately triggering the recruitment of human osteoblast cells and promoting osteogenesis.[60] Huang et al.[39] demonstrated that treating with Mg^{2+} activated the canonical Wnt signaling pathway in bone marrow stromal cells (BMSCs), resulting in

https://doi.org/10.1021/acsomega.4c04898
ACS Omega 2025, 10, 215−229

an increased expression of β-catenin. Most importantly, various studies have demonstrated the synergistic effect of Sr^{2+} and Mg^{2+} on the activation of the PI3K/Akt pathway. This activation not only bolsters osteogenesis but also effectively promotes bone formation and angiogenesis. With these considerations in mind, the results obtained herein clearly demonstrate that the addition of Sr and Mg successfully modified the 45S5 BG.

3. CONCLUSIONS

A novel bioactive glass doped with magnesium−strontium (BGMSN) was prepared from 45S5 bioactive glass (BG), strontium oxide, and magnesium oxide using a classic melt-quenching approach. The binary doping of this material resulted in good biocompatibility, excellent antibacterial properties, and a good osteogenic induction ability. Specifically, the BGMSN enhanced L-929 cell and HGF-1 cell proliferation, indicating good cellular compatibility. In addition, *in vitro* experiments confirmed that the prepared BGMSN upregulated osteogenesis-related genes in MC3T3-E1 cells, exhibiting good osteogenic bioactivity. Importantly, *in vivo* experiments performed using a rat critical-size calvarial defect model confirmed the *in vitro* results. Rats in the BGMSN treatment group exhibited a greater degree of new bone formation at the site of the calvarial defect (cf. 45S5 treatment group), confirming that BGMSN exhibited superior osteogenic potential. Notably, the excellent antibacterial properties of BGMSN provided a safe environment for bone integration. It is speculated that the mechanism of bacterial action involves the leaching of ions from the BGMSN structure to increase the pH and osmotic pressure of the medium, thereby creating an environment that is not conducive to bacterial proliferation. However, this viewpoint must be validated by future studies. Overall, the prepared BGMSN appears to be a promising multifunctional bone substitute that provides a useful reference for treating bone defects and infections. Moreover, BG exhibits excellent antibacterial properties, especially against *S. mutans*. As regards future research in this area, the role of the BGMSN in preventing dental caries warrants investigation.

4. METHODS

4.1. Preparation and Characterizations of the BGMSN. The composition of BGMSN is reported in Table S1. Commercial raw powders, namely, SiO_2, $Ca_3(PO_4)_2$, $SrCO_3$, $MgCO_3$, $CaCO_3$, and Na_2CO_3 (Carlo Erba Reagents, Italy), were mixed in a lab shaker for 2 h. Then, the mixed powders were then melted in a Pt crucible in air to produce BGMSN via a melt-quenching route, as described elsewhere. The thermal cycle to melt BGMSN was: (I) 25 °C → 1100 °C, rate 10 °C/min; (II) decarbonation step: 1100 °C for 2 h; (III) 1100 °C → 1450 °C, rate 10 °C/min; (IV) 1450 °C for 45 min. The molten glass was then quickly quenched in water (at 25 °C) to obtain a frit. The frit was dried at 110 °C for 14 h and sieved with 75 μm sieve to obtain BGMSN.[61] The morphologies of BGMSN were observed by SEM combined with EDS. The phase compositions of the samples were examined using XRD, and their functional groups were investigated using FTIR spectroscopy.

4.2. Evaluation of the Physicochemical Properties of the BGMSN. Ethylene glycol contact angles and water contact angles of BGMSN and 45S5 bioactive glasses were measured using a contact angle-measuring instrument (SZ-CAM) to calculate the surface free energy of BGMSN and 45S5 substrates according to a previous study.[23] The surface morphology of the materials was determined using an Atomic Force Microscope. Detailed procedures are provided in the Supporting Information. The *in vitro* mineralization characteristics of the BGMSN were evaluated using the SBF method according to the Kokubo protocol.[31]

4.3. Mineralization of BGMSN in SBF at Different pH Levels. The pH of the SBF was adjusted to 8.9 by utilizing either a 1 M NaOH solution or a 1 M HCl solution. After 1, 3, 5, and 7 days of immersion in SBF, BGMSN and 45S5 BG were gently rinsed three times with sterile distilled water and washed once with acetone. Biomimetic apatite formation was observed by using field-emission SEM combined with EDS, and the surface functional groups were determined by using FTIR spectroscopy.

4.4. Ion Release. The concentrations of Ca, P, Sr, and Mg ions in the SBF at pH 7.4 and 8.9 during incubation at 37 °C were also measured with the ICP-AES. Each solution with a different pH and incubation time was poured into a centrifuge tube and centrifuged at 4640*g* for 5 min. The dispersed precipitates in the supernatant were removed by filtration through a microfilter (pore size, 0.22 μm, Millipore) and the clear filtrate was collected in a tube and diluted with ultrapure water. Once 10-fold diluted solutions were preserved at 4 °C before measurement, 500-fold diluted solutions were measured via ICP-AES.[32]

4.5. Cell Cultures. The biological performance of the BGMSN material was investigated using L-929, HGF-1, and MC3T3-E1 cells, as described in the Supporting Information.

4.6. Microbiological Evaluations. The antibacterial properties of the BGMSN were evaluated using *S. aureus*, *E. coli*, and *S. mutans* as representative bacteria. The detailed procedures are described in the Supporting Information.

4.7. Animal Experiments. Male Sprague−Dawley (SD) rats, aged 6 weeks and weighing 200−250 g, were supplied by the Laboratory Animal Center of Lanzhou University. The detailed procedures are described in the Supporting Information. The animal experiments were approved and performed in accordance with the guidelines established by the Medical Laboratory Center of Lanzhou University. The experimental animal ethics approval number is LZUKQ-2023-016.

4.8. Evaluation of Osteogenesis *In Vivo*. The calvarial tissues of SD rats were visualized using a micro-CT scanner with a resolution of 18 μm for the analysis of bone regeneration. Following 3D reconstruction, the BMD, BV/TV, and trabecular thickness values were determined for the defects by using CT analysis software. The image reconstruction software NRecon 2.2, 3D reconstruction software CTvox 2.1, and CTAn 1.1 were used to analyze the microstructural parameters of the bone tissue in the modeling defect area. The analysis ranges of all of the specimens remained the same.

4.9. Histopathological Assessments. H&E and Masson's trichrome staining techniques were used to assess the formation of novel bone tissue and collagen. All samples were subjected to immunohistochemical staining for BMP-2, RUNX2, and the OPN. The detailed procedures are described in the Supporting Information.

4.10. *In Vivo* Toxicity Detections. The principal organs (heart, liver, spleen, lungs, and kidneys) from the BGMSN, 45S5, and blank control groups were collected and preserved

https://doi.org/10.1021/acsomega.4c04898
ACS Omega 2025, 10, 215−229

in 4% neutral paraformaldehyde. H&E staining was used to assess toxicity. Any abnormalities in major organs were analyzed.

4.11. Statistical Analyses. All quantitative data were expressed as means and standard deviations. Significant differences between groups were determined using one-way analysis of variance (ANOVA). SPSS software (version 27.0, IBM) was utilized for all statistical analyses. Statistical significance was set at $P < 0.05$.

■ ASSOCIATED CONTENT

Supporting Information

The Supporting Information is available free of charge at https://pubs.acs.org/doi/10.1021/acsomega.4c04898.

Additional experimental details, materials, and methods, including physicochemical properties and biocompatibility evaluation of BGMSN (PDF)

■ AUTHOR INFORMATION

Corresponding Authors

Bo Li − *State Key Laboratory of Military Stomatology, Department of Oral Implants, School of Stomatology, The Fourth Military Medical University, Xi'an 710032, China*; Email: 781552394@qq.com

Jun Hai − *CAS Key Laboratory of Chemistry of Northwestern Plant Resources and Key Laboratory of Natural Medicine of Gansu Province, Lanzhou Institute of Chemical Physics, Chinese Academy of Sciences, Lanzhou 730000, China*; orcid.org/0000-0002-7466-4649; Email: haijun@licp.cas.cn

Baoping Zhang − *School of Stomatology, Lanzhou University, Lanzhou 730000, China; Key Laboratory of Mechanics on Disaster and Environment in Western China, Ministry of Education, Lanzhou University, Lanzhou 730000, China; Institute of Biomechanics and Medical Engineering, Lanzhou University, Lanzhou 730000, China*; orcid.org/0009-0001-0736-4750; Email: zhbaoping@hotmail.com

Authors

Zhige Li − *School of Stomatology, Lanzhou University, Lanzhou 730000, China*

Ziyuan Li − *School of Stomatology, Lanzhou University, Lanzhou 730000, China*

Jiao Wang − *School of Stomatology, Lanzhou University, Lanzhou 730000, China*

Lingzi Liao − *School of Stomatology, Lanzhou University, Lanzhou 730000, China*

Xinjie Li − *School of Stomatology, Lanzhou University, Lanzhou 730000, China*

Zhidong Zhang − *School of Stomatology, Lanzhou University, Lanzhou 730000, China*

Xin Yang − *School of Stomatology, Lanzhou University, Lanzhou 730000, China*

Xiangxue Yu − *School of Stomatology, Lanzhou University, Lanzhou 730000, China*

Baoquan Fan − *School of Stomatology, Lanzhou University, Lanzhou 730000, China*

Complete contact information is available at: https://pubs.acs.org/10.1021/acsomega.4c04898

Author Contributions

#Zhige Li, Ziyuan Li, and J.W. contributed equally to this work. Conceptualization: Zhige Li, J.W. and B.Z.; Investigation: Ziyuan Li, X. Yu, and B.F.; Formal Analysis: L.L., X. Yang, Z.Z., and X.L.; Writing—Original Draft: J.W., Ziyuan Li, and X.Y.; Writing—Review & Editing: B.L., J.H., and B.Z.

Funding

The work was supported by National Natural Science Foundation of China (81970976, 21904052); National Natural Science Foundation of Gansu Province (23JRRA1080, 20JR10RA641); and Fundamental Research Funds for the Scientific Research Fund of School (Hospital) of Stomatology Lanzhou University ((22)0660; lzukqky-2022-t12; lzukqky-2022-t16).

Notes

The authors declare no competing financial interest.

■ ACKNOWLEDGMENTS

We thank all individuals who participated in this study.

■ REFERENCES

(1) Wei, H.; Cui, J.; Lin, K.; Xie, J.; Wang, X. Recent Advances in Smart Stimuli-Responsive Biomaterials for Bone Therapeutics and Regeneration. *Bone Res.* **2022**, *10* (1), 17.

(2) Li, R.; Qiu, S.; Yang, W.; Rao, Z.; Chen, J.; Yang, Y.; Zhu, Q.; Liu, X.; Bai, Y.; Quan, D. A Comparative Study of Human and Porcine-derived Decellularised Nerve Matrices. *Biomater. Transl.* **2023**, *4* (3), 180−195.

(3) Liu, H.; Zhang, H.; Wang, S.; Cui, J.; Weng, W.; Liu, X.; Tang, H.; Hu, Y.; Li, X.; Zhang, K.; Zhou, F.; Jing, Y.; Su, J. Bone-targeted Bioengineered Bacterial Extracellular Vesicles Delivering siRNA to Ameliorate Osteoporosis. *Composites, Part B* **2023**, *255*, 110610.

(4) Wang, M.; Wu, Y.; Li, G.; Lin, Q.; Zhang, W.; Liu, H.; Su, J. Articular Cartilage Repair Biomaterials: Strategies and Applications. *Mater. Today Bio* **2024**, *24*, 100948.

(5) Wang, X.; Li, Q.; Yang, H. Effect of Radiation Sterilisation on the Structure and Antibacterial Properties of Antimicrobial Peptides. *Biomater. Transl.* **2023**, *4* (1), 51−61.

(6) Bose, S.; Bhattacharjee, A.; Banerjee, D.; Boccaccini, A. R.; Bandyopadhyay, A. Influence of Random and Designed Porosities on 3D Printed Tricalcium Phosphate-bioactive Glass Scaffolds. *Addit. Manuf.* **2021**, *40*, 101895.

(7) Zhu, S.; Li, M.; Wang, Z.; Feng, Q.; Gao, H.; Li, Q.; Chen, X.; Cao, X. Bioactive Glasses-Based Nanozymes Composite Macroporous Cryogel with Antioxidative, Antibacterial, and Pro-Healing Properties for Diabetic Infected Wound Repair. *Adv. Healthcare Mater.* **2023**, *12* (29), 2302073.

(8) Wei, S.; Ma, J.-X.; Xu, L.; Gu, X.-S.; Ma, X.-L. Biodegradable Materials for Bone Defect Repair. *Mil. Med. Res.* **2020**, *7* (1), No. 54, DOI: 10.1186/s40779-020-00280-6.

(9) Chen, M.; Li, Y.; Hou, W.-X.; Peng, D.-Y.; Li, J. K.; Zhang, H.-X. The Antibacterial Effect, Biocompatibility, and Osteogenesis of Vancomycin-Nanodiamond Composite Scaffold for Infected Bone Defects. *Int. J. Nanomed.* **2023**, *18*, 1365−1380.

(10) Ji, H.; Shen, G.; Liu, H.; Liu, Y.; Qian, J.; Wan, G.; Luo, E. Biodegradable Zn-2Cu-0.5Zr Alloy Promotes the Bone Repair of Senile Osteoporotic Fractures Via the Immune-modulation of Macrophages. *Bioact. Mater.* **2024**, *38*, 422−437.

(11) Feng, P.; He, R.; Gu, Y.; Yang, F.; Pan, H.; Shuai, C. Construction of Antibacterial Bone Implants and Their Application in Bone Regeneration. *Mater. Horiz.* **2024**, *11* (3), 590−625.

(12) Bellucci, D.; Veronesi, E.; Dominici, M.; Cannillo, V. A New Bioactive Glass with Extremely High Crystallization Temperature and Outstanding Biological Performance. *Mater. Sci. Eng. C.* **2020**, *110*, No. 110699.

(13) Tao, R.; Mi, B.; Hu, Y.; Lin, S.; Xiong, Y.; Lu, X.; Panayi, A. C.; Li, G.; Liu, G. Hallmarks of Peripheral Nerve Function in Bone Regeneration. *Bone Res.* **2023**, *11* (1), 6.
(14) Weng, Y.; Jian, Y.; Huang, W.; Xie, Z.; Zhou, Y.; Pei, X. Alkaline Earth Metals for Osteogenic Scaffolds: From Mechanisms to Applications. *J. Biomed. Mater. Res., Part B.* **2023**, *111*, 1447−1474.
(15) Zhou, H.; Liang, B.; Jiang, H.; Deng, Z.; Yu, K. Magnesium-based Biomaterials as Emerging Agents for Bone Repair and Regeneration: From Mechanism to Application. *J. Magn. Alloys.* **2021**, *9*, 779−804.
(16) Huang, Y. Z.; Wang, J. J.; Huang, Y. C.; Wu, C. G.; Zhang, Y.; Zhang, C. L.; Bai, L.; Xie, H. Q.; Li, Z. Y.; Deng, L. Organic Composite-Mediated Surface Coating of Human Acellular Bone Matrix with Strontium. *Mater. Sci. Eng. C.* **2018**, *84*, 12−20.
(17) Bulina, N. V.; Vinokurova, O. B.; Prosanov, I. Y.; Vorobyev, A. M.; Gerasimov, K. B.; Borodulina, I. A.; Pryadko, A.; Botvin, V. V.; Surmeneva, M. A.; Surmenev, R. A. Mechanochemical Synthesis of Strontium- and Magnesium-substituted and Cosubstituted Hydroxyapatite Powders for a Variety of Biomedical Applications. *Ceram. Int.* **2022**, *48* (23), 35217−35226.
(18) Liu, X.; Sun, Y.; Shen, J.; Min, H. S.; Xu, J.; Chai, Y. Strontium Doped Mesoporous Silica Nanoparticles Accelerate Osteogenesis and Angiogenesis in Distraction Osteogenesis by Activation of Wnt Pathway. *Nanomed.: Nanotechnol., Biol. Med.* **2022**, *41*, No. 102496.
(19) Silva, A. V.; Gomes, D. d. S.; Victor, R. d. S.; Santana, L. N. d. L.; Neves, G. A.; Menezes, R. R. Influence of Strontium on the Biological Behavior of Bioactive Glasses for Bone Regeneration. *Materials.* **2023**, *16*, 7654.
(20) Anwar, A.; Kanwal, Q.; Sadiqa, A.; Razaq, T.; Khan, I. H.; Javaid, A.; Khan, S.; Tag-Eldin, E.; Ouladsmane, M. Synthesis and Antimicrobial Analysis of High Surface Area Strontium-Substituted Calcium Phosphate Nanostructures for Bone Regeneration. *Int. J. Mol. Sci.* **2023**, *24* (19), 14527.
(21) Nagyné-Kovács, T.; Studnicka, L.; Kincses, A.; Spengler, G.; Molnar, M.; Tolner, M.; Lukacs, I. E.; Szilagyi, I. M.; Pokol, G. Synthesis and Characterization of Sr and Mg-Doped Hydroxyapatite by a Simple Precipitation Method. *Ceram. Int.* **2018**, *44* (18), 22976−22982.
(22) Yu, S.; Sun, T.; Liu, W.; Yang, L.; Gong, H.; Chen, X.; Li, J.; Weng, J. PLGA Cage-Like Structures Loaded with Sr/Mg-Doped Hydroxyapatite for Repairing Osteoporotic Bone Defects. *Macromol. Biosci.* **2022**, *22* (8), No. 2270023.
(23) Xu, K.; Mu, C.; Zhang, C.; Deng, S.; Lin, S.; Zheng, L.; Chen, W.; Zhang, Q. Antioxidative and Antibacterial Gallium (III)-phenolic Coating for Enhanced Osseointegration of Titanium Implants via Pro-osteogenesis and Inhibiting Osteoclastogenesis. *Biomaterials.* **2023**, *301*, 122268.
(24) Chou, Y. F.; Chiou, W. A.; Xu, Y. H.; Dunn, J. C. Y.; Wu, B. M. The Effect of pH on the Structural Evolution of Accelerated Biomimetic Apatite. *Biomaterials.* **2004**, *25* (22), 5323−5331.
(25) Besleaga, C.; Nan, B.; Popa, A.-C.; Balescu, L. M.; Nedelcu, L.; Neto, A. S.; Pasuk, I.; Leonat, L.; Popescu-Pelin, G.; Ferreira, J. M. F.; Stan, G. E. Sr and Mg Doped Bi-Phasic Calcium Phosphate Macroporous Bone Graft Substitutes Fabricated by Robocasting: A Structural and Cytocompatibility Assessment. *J. Funct. Biomater.* **2022**, *13* (3), No. 123.
(26) Dabare, P. R. L.; Bachhuka, A.; Quek, J. Y.; Marsal, L. F. F.; Hayball, J.; Vasilev, K. Nano-Roughness-Mediated Macrophage Polarization for Desired Host Immune Response. *Small Sci.* **2023**, *3* (10), No. 2300080, DOI: 10.1002/smsc.202300080.
(27) Jones, J. R. Reprint of: Review of bioactive glass: From Hench to hybrids. *Acta Biomater.* **2015**, *23*, S53−S82.
(28) Pan, S.; Yin, J.; Yu, L.; Zhang, C.; Zhu, Y.; Gao, Y.; Chen, Y. 2D MXene-Integrated 3D-Printing Scaffolds for Augmented Osteosarcoma Phototherapy and Accelerated Tissue Reconstruction. *Adv. Sci.* **2020**, *7* (2), No. 1901511, DOI: 10.1002/advs.201901511.
(29) Khang, D.; Kim, S. Y.; Liu-Snyder, P.; Palmore, G. T. R.; Durbin, S. M.; Webster, T. J. Enhanced Fibronectin Adsorption on Carbon Nanotube/poly(carbonate) Urethane: Independent Role of Surface Nano-roughness and Associated Surface Energy. *Biomaterials.* **2007**, *28* (32), 4756−4768.
(30) Jones, J. R. Review of Bioactive Glass: From Hench to Hybrids. *Acta Biomater.* **2013**, *9*, 4457−4486.
(31) Zamani, D.; Mortarzadeh, F.; Bizari, D. Alginate-Bioactive Glass Containing Zn and Mg Composite Scaffolds for Bone Tissue Engineering. *Int. J. Biol. Macromol.* **2019**, *137*, 1256−1267.
(32) Vecchio, G.; Darcos, V.; Grill, S. L.; Brouillet, F.; Coppel, Y.; Duttine, M.; Soulié, J.; et al. Spray-dried Ternary Bioactive Glass Microspheres: Direct and Indirect Structural Effects of Copper-doping on Acellular Degradation Behavior. *Acta Biomater.* **2024**, *181*, 453−468.
(33) Jiang, H.; Ochoa, M.; Waimin, J. F.; Rahimi, R.; Ziaie, B. A pH-regulated Drug Delivery Dermal Patch for Targeting Infected Regions in Chronic Wounds. *Lab Chip.* **2019**, *19* (13), 2265−2274.
(34) Cui, T.; Yu, J.; Wang, C. F.; Chen, S.; Li, Q.; Guo, K.; Ren, J.; et al. Micro-Gel Ensembles for Accelerated Healing of Chronic Wound via pH Regulation. *Adv. Sci.* **2022**, *9* (22), No. 2201254, DOI: 10.1002/advs.202201254.
(35) Ibrahim, H. M.; Klingner, A. A review on Electrospun Polymeric Nanofibers: Production Parameters and Potential Applications. *Polym. Test.* **2020**, *90*, 106647.
(36) Angel, N.; Li, S.; Kong, L. Emerging Applications of Nanofibers Electrospun from Carbohydrate Polymers. *J. Future Foods.* **2024**, *4* (4), 289−299.
(37) Vecchio, G.; Darcos, V.; Grill, S. L.; Brouillet, F.; Coppel, Y.; Duttine, M.; Pugliara, A.; Combes, C.; Soulié, J. Spray-dried Ternary Bioactive Glass Microspheres: Direct and Indirect Structural Effects of Copper-doping on Acellular Degradation Behavior. *Acta Biomater.* **2024**, *181*, 453−468.
(38) Hou, H.-H.; Lee, B.-S.; Liu, Y.-C.; Wang, Y.-P.; Kuo, W.-T.; Chen, I. H.; He, A.-C.; Lai, C.-H.; Tung, K.-L.; Chen, Y.-W. Vapor-Induced Pore-Forming Atmospheric-Plasma-Sprayed Zinc-, Strontium-, and Magnesium-Doped Hydroxyapatite Coatings on Titanium Implants Enhance New Bone Formation—An In Vivo and In Vitro Investigation. *Int. J. Mol. Sci.* **2023**, *24* (5), No. 4933.
(39) Weng, Y.; Jian, Y.; Huang, W.; Xie, Z.; Zhou, Y.; Pei, X. Alkaline earth metals for osteogenic scaffolds: From mechanisms to applications. *J. Biomed. Mater. Res., Part B.* **2023**, *111* (7), 1447−1474.
(40) Chaichana, W.; Insee, K.; Chanachai, S.; Benjakul, S.; Aupaphong, V.; Naruphontjirakul, P.; Panpisut, P. Physical/Mechanical and Antibacterial Properties of Orthodontic Adhesives Containing Sr-bioactive Glass Nanoparticles, Calcium Phosphate, and Andrographolide. *Sci. Rep.* **2022**, *12*, No. 6635, DOI: 10.1038/s41598-022-10654-6.
(41) Yun, H. M.; Lee, J. Y.; Kim, S. H.; Kwon, I. K.; Park, K. R. Effects of Triterpene Soyasapogenol B from Arachis hypogaea (Peanut) on Differentiation, Mineralization, Autophagy, and Necroptosis in Pre-Osteoblasts. *Int. J. Mol. Sci.* **2022**, *23* (15), No. 8297.
(42) Yu, X.; Wang, X.; Li, D.; Sheng, R.; Qian, Y.; Zhu, R.; Wang, X.; Lin, K. Mechanically Reinforced Injectable Bioactive Nanocomposite Hydrogels for In-situ Bone Regeneration. *Chem. Eng. J.* **2022**, *433*, 132799.
(43) Gavinho, S. R.; Pádua, A. S.; Holz, L. I. V.; Sá-Nogueira, I.; Silva, J. C.; Borges, J. P.; Valente, M. A.; Graça, M. P. F. Bioactive Glasses Containing Strontium or Magnesium Ions to Enhance the Biological Response in Bone Regeneration. *Nanomaterials.* **2023**, *13*, 2717.
(44) Nabiyouni, M.; Brückner, T.; Zhou, H.; Gbureck, U.; Bhaduri, S. B. Magnesium-based Bioceramics in Orthopedic Applications. *Acta Biomater.* **2018**, *66*, 23−43.
(45) Riddle, R. C.; Taylor, A. F.; Genetos, D. C.; Donahue, H. J. MAP Kinase and Calcium Signaling Mediate Fluid Flow-induced Human Mesenchymal Stem Cell Proliferation. *Am. J. Physiol. − Cell Physiol.* **2006**, *290* (3), C776−C784.
(46) Hoppe, A.; Gueldal, N. S.; Boccaccini, A. R. A Review of the Biological Response to Ionic Dissolution Products from Bioactive Glasses and Glass-ceramics. *Biomaterials.* **2011**, *32* (11), 2757−2774.

https://doi.org/10.1021/acsomega.4c04898
ACS Omega 2025, 10, 215−229

(47) O'Neill, E.; Awale, G.; Daneshmandi, L.; Umerah, O.; Lo, K. W. H. The Roles of Ions on Bone Regeneration. *Drug Discovery Today*. **2018**, *23* (4), 879−890.
(48) Xue, Y.; Zhang, L.; Liu, F.; Zhao, Y.; Zhou, J.; Hou, Y.; Bao, H.; Kong, L.; Ma, F.; Han, Y. Surface Bandgap Engineering of Nanostructured Implants for Rapid Photothermal Ion Therapy of Bone Defects. *Adv. Healthcare Mater.* **2022**, *11* (22), No. 2200998.
(49) Howden, B. P.; Giulieri, S. G.; Lung, T. W. F.; Baines, S. L.; Sharkey, L. K.; Lee, J. Y. H.; Hachani, A.; Monk, I. R.; Stinear, T. P. Staphylococcus Aureus Host Interactions and Adaptation. *Nat. Rev. Microbiol.* **2023**, *21* (6), 380−395.
(50) Ge, X.; Ren, C. Z.; Ding, Y. H.; Chen, G.; Lu, X.; Wang, K. F.; Ren, F. Z.; Yang, M.; Wang, Z. C.; Li, J. L.; An, X. X.; Qian, B.; Leng, Y. Micro/Nano-Structured TiO_2 Surface with Dual-Functional Antibacterial Effects for Biomedical Applications. *Bioact. Mater.* **2019**, *4*, 346−357.
(51) Luo, J. Y.; Feng, Z. N.; Lyu, X.; Zhang, L. L. Novel Lactotransferrin-Derived Antimicrobial Peptide LF-1 Inhibits the Cariogenic Virulence Factors of Streptococcus Mutans. *Antibiotics.* **2023**, *12* (3), 563.
(52) Baheiraei, N.; Eyni, H.; Bakhshi, B.; Najafloo, R.; Rabiee, N. Effects of Strontium Ions with Potential Antibacterial Activity on in Vivo Bone Regeneration. *Sci. Rep.* **2021**, *11*, No. 8745, DOI: 10.1038/s41598-021-88058-1.
(53) Zamani, D.; Moztarzadeh, F.; Bizari, D. Alginate-bioactive Glass Containing Zn and Mg Composite Scaffolds for Bone Tissue Engineering. *Int. J. Biol. Macromol.* **2019**, *137*, 1256−1267.
(54) He, F.; Lu, T.; Fang, X.; Qiu, C.; Tian, Y.; Li, Y.; Zuo, F.; Ye, J. Study on MgxSr3-x(PO4)2 Bioceramics as Potential Bone Grafts. *Colloids Surf., B.* **2019**, *175*, 158−165.
(55) Dorogin, J.; Hochstatter, H. B.; Shepherd, S. O.; Svendsen, J. E.; Benz, M. A.; Powers, A. C.; Fear, K. M.; Townsend, J. M.; Prell, J. S.; Hosseinzadeh, P.; Hettiaratchi, M. H. Moderate-Affinity Affibodies Modulate the Delivery and Bioactivity of Bone Morphogenetic Protein-2. *Adv. Healthcare Mater.* **2023**, *12* (26), No. 2300793.
(56) Hu, G. L.; Yu, Y. L.; Sharma, D.; Pruett-Miller, S. M.; Ren, Y. S.; Zhang, G. F.; Karner, C. M. Glutathione Limits RUNX2 Oxidation and Degradation to Regulate Bone Formation. *JCI Insights.* **2023**, *8* (16), No. 166888.
(57) Cianferotti, L.; Gomes, A. R.; Fabbri, S.; Tanini, A.; Brandi, M. L. The Calcium-Sensing Receptor in Bone Metabolism: From Bench to Bedside and Back. *Osteoporosis Int.* **2015**, *26* (8), 2055−2071.
(58) Cai, J. Y.; Zhang, Q. Q.; Chen, J. B.; Jiang, J.; Mo, X. M.; He, C. L.; Zhao, J. Z. Electrodeposition of Calcium Phosphate onto Polyethylene Terephthalate Artificial Ligament Enhances Graft-bone Integration after Anterior Cruciate Ligament Reconstruction. *Bioact. Mater.* **2021**, *6* (3), 783−793.
(59) Manoochehri, H.; Ghorbani, M.; Moosazadeh Moghaddam, M.; Nourani, M. R.; Makvandi, P.; Sharifi, E. Strontium Doped Bioglass Incorporated Hydrogel-based Scaffold for Amplified Bone Tissue Regeneration. *Sci. Rep.* **2022**, *12*, No. 10160, DOI: 10.1038/s41598-022-14329-0.
(60) Hu, J.; Shao, J.; Huang, G.; Zhang, J.; Pan, S. In Vitro and in Vivo Applications of Magnesium-enriched Biomaterials for Vascularized Osteogenesis in Bone Tissue Engineering: A Review of Literature. *J. Funct. Biomater.* **2023**, *14*, 326.
(61) Sergi, R.; Bellucci, D.; Salvatori, R.; Anesi, A.; Cannillo, V. A Novel Bioactive Glass Containing Therapeutic Ions with Enhanced Biocompatibility. *Materials.* **2020**, *13* (20), No. 4600.

https://doi.org/10.1021/acsomega.4c04898
ACS Omega 2025, 10, 215−229